

OPTICAL–NIR COLOR GRADIENTS IN EARLY TYPE GALAXIES AT $Z \lesssim 1.0^1$ SASHA HINKLEY², MYUNGSHIN IM³
Draft version December 1, 2018

ABSTRACT

Recent studies based on line indices of nearby early-type galaxies suggest that stars in the galaxies' inner part may be younger and more metal rich than stars in the outer part. If confirmed, the finding has a profound implication for the formation and evolution of early-type galaxies, since such age gradients naturally arise if merging played an important role in their formation/evolution. As an independent test for the existence of the age gradient, we investigate the optical-NIR color gradients of six field early-type galaxies at $z \simeq 0.4 - 1.0$ where the age gradient is expected to be detectable when combined with $z = 0$ calibrations. By utilizing HST NICMOS H-band imaging along with WFPC2 optical data, we obtain a broad wavelength baseline, giving results that are sensitive to the expected age gradient. When compared with simple model predictions, five of the objects show negligible age gradients and are metallicity gradient dominated, while the remaining object shows a color gradient consistent with the age+metallicity gradient picture. Our results suggest that stars within early-type galaxies may be coeval at $z \sim 1$, but sprinkling of young stars might have occurred at $z < 1$.

Subject headings: cosmology: observations – galaxies: elliptical and lenticular, cD – galaxies: evolution

1. INTRODUCTION

Early-type galaxies in the local universe show a moderate change in stellar populations from their centers toward their edges. Stars are redder toward the center of early-types (e.g., Franx & Illingworth 1990; Peletier *et al.* 1990a, 1990b; Kormendy & Djorgovski 1989), and studies of metallicity-sensitive line indices of nearby ellipticals (e.g., Kobayashi & Arimoto 1999; Gonzalez 1993; Carollo *et al.* 1993) show that a change in metallicity has a substantial effect on the color gradient. However, when age-sensitive Balmer line indices (see Worthey 1994) are investigated, some ellipticals not only show metallicity gradients, but also age gradients in which the inner part is younger than the outer part of the galaxy (Gonzalez 1993; Tantalo, Chiosi, & Bressan 1998; Trager *et al.* 2000).

This picture of an age+metallicity gradient makes sense if mergers play a significant role in the formation/evolution of early-type galaxies. Only the metallicity gradient is expected in models where early-type galaxies formed via monolithic collapse at high redshift and evolved passively thereafter (e.g., Carlberg 1984). The indication of younger stars near the center suggests additional star formation/accretion activities very possibly through merging. However, a number of studies point out difficulties of using Balmer lines for age measurements (Maraston & Thomas 2000; Bressan *et al.* 1996; Lee, Yoon, & Lee 2001; Jorgensen 1997; Fisher, Franx, & Illingworth 1995) — thus, an independent assessment of the age+metallicity gradient model is highly desired.

One promising way to detect age gradients is to study color gradients of distant early-type galaxies ($z \gtrsim 0.2$). As one looks back in time, younger stars become more visible out of old stars where they are embedded. Therefore, the inner parts of distant early-type galaxies would

look as blue as, or bluer than, the outer region if the age+metallicity gradient model is correct. Consequently, the color gradient would become flatter or even reversed as a function of redshift.

Color gradients of distant early-types have been studied using optical HST images, and such studies have excluded models where the color gradient is driven purely by age (Tamura *et al.* 2001; Saglia *et al.* 2000). However, they put few constraints on the more plausible age+metallicity gradient model, due to the fact that the age effect, when buried under the metallicity gradient, is barely detectable in observed optical passbands (see section 5). Several studies find E/S0 candidates with bluer cores (e.g., Abraham *et al.* 1999; Menanteau *et al.* 2001; Im *et al.* 2001a), but a detailed study of their kinematic and structural properties shows that these galaxies do not appear to evolve into typical E/S0s today (Im *et al.* 2001b).

In an attempt to test the age+metallicity gradient model, we have studied optical-NIR (near-infrared) color gradients of early-type galaxies out to $z \sim 1$, using HST NICMOS data for NIR and HST WFPC2 data for optical. In this paper, we present our preliminary results which favor no significant age-gradient in the majority of early-type galaxies in our sample.

2. SAMPLE

Our sample consists of six field E/S0 galaxies at $z \lesssim 1$ of which five are located in the Groth strip (Rhodes *et al.* 2001), and one from the Hawaii Deep Field (Cowie *et al.* 1994). These objects come from the NICMOS snapshot survey of distant galaxies (HST GO7895 program). The snapshot survey obtained HST NICMOS Camera 2 *H*-band data (F160W, exposure time of 1200 secs per object) of 16 field galaxies at $0.2 \lesssim z \lesssim 1$ for which redshifts

¹ Based on observations with the NASA/ESA *Hubble Space Telescope*, obtained at the Space Telescope Science Institute, which is operated by the Association of Universities for Research in Astronomy, Inc., under NASA contract NAS5-26555.

² Physics Department, University of California, Santa Cruz, CA 95064; shinkley@ucolick.org

³ Astronomy & Astrophysics Department, University of California, Santa Cruz, CA 95064; myung@ucolick.org

as well as HST optical data are available in V (F606W) and/or I (F814W) bands.

E/S0 galaxies are chosen using the quantitative selection criteria of Im *et al.* (2001a; 2001b) imposed on the I -band data. The method uses two parameters: bulge-to-total light ratio (B/T) which measures the significance of the bulge component, and the residual parameter (R) which measures the smoothness and symmetry of the galaxy. We adopt $B/T \geq 0.4$ and $R \leq 0.08$ following Im *et al.* (2001a). Note that these parameters are derived for each galaxy in the Groth strip using the 2-dimensional surface brightness fitting algorithm, GIM2D (Simard *et al.* 2001), which also returns other parameters such as the half light radius (r_{hl}). For one galaxy in the Hawaii Deep Field, the B/T value is taken from the MDS database (Ratnatunga, Ostrander, & Griffiths 1999). Although an R value is not readily available for this object, a visual inspection confirms that it is an E/S0. The basic data for our sample are presented in Table 1, and images are shown in Fig. 1. Note that magnitudes are in the Vega system for the HST filters (Holtzman *et al.* 1995; Simard *et al.* 2001).

3. DATA REDUCTION AND ANALYSIS

The reduction of the H -band data was performed using the IRAF⁴ NICPROTO package (Bushouse *et al.* 2000). The NICPROTO package⁵ includes the standard NICMOS pipeline procedure (calnica and calnichb), but it gives special attention to removing image anomalies such as a pedestal variation across the array and a varying bias sensitivity in the detector itself. In addition, all of the data were reduced using the new NICMOS synthetic dark frames, which helped to alleviate a time-dependent shading feature caused by the readout amplifiers (Monroe & Bergeron 1999). We have carried out these additional reduction procedures in order to remove the background variation as much as possible, since color gradient measurements require very careful background determination.

Four dither exposures were obtained for each field. From these four, a single higher signal-to-noise image was produced after the four were cross-correlated and shifted using subpixel translations with cubic spline interpolation. Simulations using tinytim PSFs confirm that the simple shift-and-add method used here will not substantially change the characteristics of the NICMOS PSF. The WFPC2 images were obtained from either the DEEP or MDS databases. Once the calibration and reductions were complete, the H-band Vega magnitudes were calculated using the relation $H = 21.75 - 2.5 \log(DN/sec)$ (Schultz *et al.* 2001), where DN (counts) is obtained from GIM2D.

Since NICMOS and WFPC2 have different PSFs, we matched the PSF by cross-convolving our data – i.e., the WFPC2 images were convolved with the NICMOS PSF and vice versa. The PSFs were created at the object location using the TinyTim package (Krist 1993). Since the plate scales of the WFPC2 (0''.0996) and NICMOS Camera2 (0''.075) are different, oversampled PSFs were produced and then rebinned to have the platescale of the other detector. Note however, that no cross-convolution was performed for the ($V - I$) gradients since the difference in the V and I PSF is insignificant.

The standard IRAF photometry package “ellipse” was used to fit elliptical isophotes to each object, and care was taken to ensure that the ellipticity and position angles were consistent between the NICMOS and WFPC2 data. Moreover, each object’s isophotal centroid agreed extremely well between the two bands, and these were consistent with the GIM2D values to within 0.3 pixels.

The background value was determined by taking a median sky value of the region beyond $5 r_{hl}$ and within a 6''.4 by 6''.4 square region of the object. We checked the sky value by constructing the flux growth curve, and found that the growth curve nearly flattened out beyond $4 r_{hl}$. The sky value is consistent with the output from GIM2D which uses a similar procedure (<10%). Slight differences in sky values affect the aperture photometry at the outer part of the galaxy at $3 - 5 r_{hl}$, thus we have restricted our study to regions inside $r \lesssim 2 r_{hl}$.

4. MODELS

This study uses simplified versions of the two kinds of models discussed in section 1. The first is a pure metallicity gradient model, and the second is an age+metallicity gradient model. The metallicity (Z) and the age (t) gradients are modelled as:

$$\delta \log(Z) = C + C_Z \log(r/r_{hl}), \quad (1)$$

$$\delta \log(t) = C' + C_t \log(r/r_{hl}), \quad (2)$$

where C and C' are constants, r_{hl} is the half light radius, and C_Z and C_t are the slope of the metallicity gradient and the age gradient respectively.

The pure metallicity gradient model assumes no age gradient (i.e., $C_t = 0$), and local E/S0s show C_Z values in the range of $-0.4 \lesssim C_Z \lesssim -0.1$ with $\langle C_Z \rangle = -0.2$ (Henry & Worthey 1999; Kobayashi & Arimoto 1999). The plausible range for the central metallicity value is 100%–300% Z_{\odot} within $r_{hl}/8$ (Trager *et al.* 2001), and we use 250% Z_{\odot} for the inner region defined at $\log(\frac{r}{r_{hl}}) \simeq -1.175$ (the light-weighted mean radius within $r_{hl}/8$). The outer region is defined as where the metallicity falls to 100% Z_{\odot} . The model colors are calculated at these inner and outer radii, and the model color gradient is the straight line which connects the two points. Then, we find the best-fit C_Z and the age (or z_{for} , the formation redshift) by minimizing a χ^2 fit to the observed color gradient.

The age+metallicity gradient model assumes an age gradient in addition to the metallicity gradient. Line indices studies find that $\langle C_t \rangle \simeq 0.1$ and $\langle C_Z \rangle \simeq -0.25$ for local E/S0s (Henry & Worthey 1999). Our base age+metallicity gradient model assumes these slopes, and the zero point of the base model is adjusted to fit the optical-NIR color at $r/r_{hl} \sim 0.1 - 0.2$ by changing z_{for} . Besides the base model, we allow our model to fit for C_t , C_Z and z_{for} . Again, 250% Z_{\odot} is placed in consideration for the inner metallicity. Note that we use only two points for the color gradient predictions. Consequently, the predicted color gradients are straight lines. This should be a good first order approximation for the color gradients given the quality of our data, although the color gradients can get curved when the age effect is strong (e.g., Tamura *et al.* 2001).

⁴ IRAF is distributed by the National Optical Astronomy Observatories, under contract to AURA, Inc.

⁵ The most up-to-date NICMOS tasks in STSDAS now include most NICPROTO procedures.

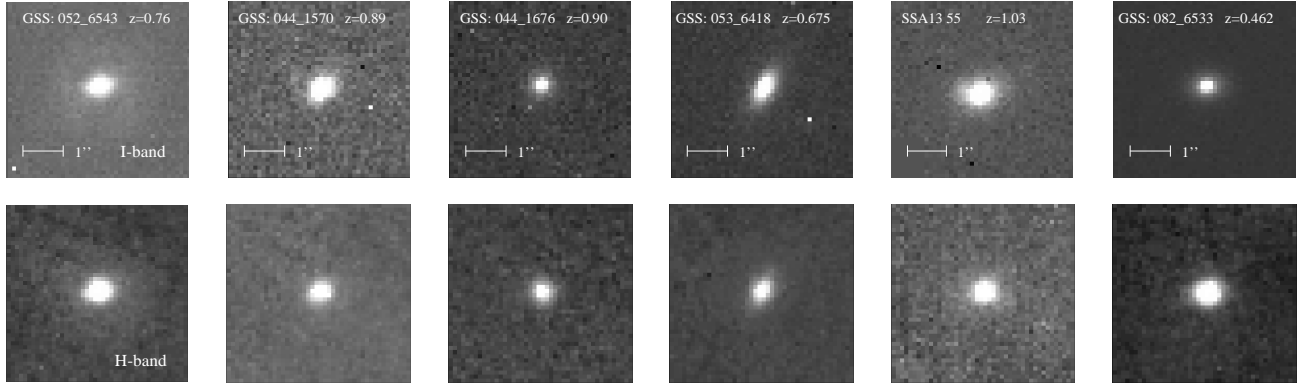


FIG. 1.— The I -band (top row) and the H -band (bottom row) images of E/S0s in our sample. All images are oriented the same way and are on the same scale.

SEDs are generated at different ages and metallicities using the 1996 version of Bruzual & Charlot model (1993). The standard Salpeter IMF, 0.1 Gyr burst, and an open universe with $\Omega_0 = 0.2$ and $H_0 = 70 \text{ km sec}^{-1}$ are assumed. The SEDs are redshifted and K -corrections are derived using the formula in Im *et al.* (1995), which are then used for calculating colors. Note that the zeropoint of the optical-NIR color may vary with spectral synthesis models, but the slope of the color gradient is not likely to be model-sensitive (Charlot, Worthey, & Bressan 1996). Also, the predicted slope of the color gradient is insensitive to the assumed cosmology.

5. RESULTS

Color gradients for our sample are shown in Fig. 2. Except for one object without V -band data, two plots are shown for each object — one for the $V - H$ gradient and another for the $V - I$ gradient. At $z = 1$, the observed $V - H$ gradient corresponds roughly to the rest-frame $U - I$ gradient. Also plotted in Fig. 2 are model predictions.

The first five objects have $V - H$ or $I - H$ gradients inconsistent with that of the base age+metallicity gradient model predictions, while their color gradients can be well matched by the pure metallicity gradient model with the best-fit slope of $C_Z = (-0.2 \sim -0.4) \pm 0.05$. Fig. 2 also demonstrates that the $V - I$ gradient is not very sensitive to the age gradient, thus not useful for testing the age+metallicity gradient model. Since these objects are already at the lookback time of ~ 7 Gyrs, the mean stellar age in the inner part must be less than a few Gyrs under the base age+metallicity gradient model. This would produce flat or reversed optical-NIR color gradients (dashed lines), which does not match the data. Thus, it is unlikely that any significant secondary star formation/accretion event occurred at the center of these galaxies before $z \sim 1$. To prove this point further, we fit the color gradient for C_t using a fixed $C_Z = -0.25$, and find no significant age gradient ($C_t \simeq 0.01 \pm 0.02$). One might consider a case where the age gradient is hidden under a steep metallicity gradient. To check such possibility, we fit for C_t using $C_Z = -0.5$ and find that $C_t \simeq 0.08 \pm 0.02$ for the five objects. The derived C_t values are inconsistent with the local constraints where $C_t \simeq 0.3$ when $C_Z \simeq -0.5$ (Henry & Worthey 1999). Thus, we still require more young stars near the center for this picture to be true. Note that the

model color is sensitive to the assumed metallicity. If one uses a different metallicity value, the zero point of the predicted color gradient shifts too. However, this shift in the zero-point can be compensated by changing z_{for} . We tried 100% Z_\odot for the metallicity of the central part. This changed the predicted color gradient slightly, but did not affect the overall conclusion about the age gradient.

The $(V - H)$ color gradient of the last object (GSS082_6533) shows that its inner part is bluer than the outer part, with the best-fit gradients being $C_Z = -0.27 \pm 0.20$ and $C_t = 0.20 \pm 0.10$. This is consistent with the age+metallicity gradient picture, and sprinkling of young, blue stars might have occurred in the past few Gyrs, near the center of this galaxy.

Fig. 2 also shows that the sensitivity to the age gradient seems to be higher for E/S0s at high- z . For example, the difference between the pure- Z model and the age+metallicity gradient models is more drastic for the $z = 0.89$ object than the $z = 0.462$ object. However, secondary star formation may occur after $z \sim 1$, in which case it is advantageous to observe galaxies at moderate z .

6. CONCLUSIONS

We have performed surface photometry on six early-type galaxies at $z = 0.4 - 1.0$ and obtained their optical-NIR color gradients. These were then compared with simple models driven purely by metallicity or models driven by changes in age *and* metallicity. The age+metallicity model predicts a flattened or reversed optical-NIR color gradient due to the assumed existence of younger stars in the inner region. However, the model fails to reproduce the observed color gradient of the majority of our galaxies (5/6). Therefore, we conclude that no significant secondary star formation/accretion occurred at $z \gtrsim 1$ for these galaxies. While evidence is lacking for a strong age-gradient for $z \sim 1$ early-types, one object at the lowest redshift ($z = 0.462$) shows a color gradient consistent with the age+metallicity gradient model. This shows that the age-gradient is detectable, and that secondary bursts/accretions may occur at moderate redshifts. In the future, we hope to draw firmer conclusions on this issue by enlarging our sample and improving our model predictions.

This work was supported by the STScI grant GO-07895.02-96A, and partial support was provided by the

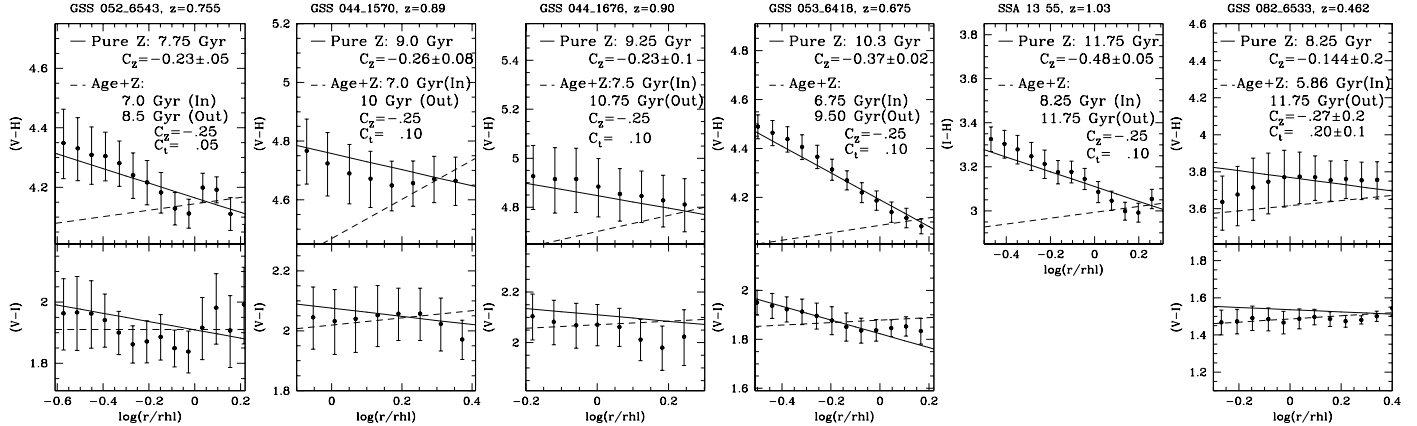


FIG. 2.— Shown here are pairs of $(V - H)$ and $(V - I)$ gradients for all of our data. Object SSA13 #55 does not have observations in V , so only an $I - H$ gradient is shown. The solid lines indicate the purely metallicity-driven model, while the dashed lines are the age + metallicity models. Also shown in the figure are the best-fit or assumed C_Z , C_t , and the age for the models. For 052.6543, a slightly shallower age gradient is used (0.05) since the canonical value produces a color gradient that is negatively too steep. For a majority of this sample (5/6), the gradients follow the purely metallicity-driven model. Only the last object, GSS 082.6533, shows a sign of young stars in its inner region. In all of the plots, the points are closely spaced, so two adjacent isophotes may share some pixels. Thus, the error bars are not independent of each other. The lookback times of 6, 7, 8, 9, and 10 Gyrs correspond to redshifts of 0.79, 1.1, 1.5, 2.2, and 3.4 respectively.

NSF grant AST-9529098. This project greatly benefitted from the help and comments provided by Luc Simard, Sandra Faber, David Koo, Dan Magee and Rychard Bouwens. We also acknowledge the use of the data from the DEEP

project, which was funded by the NSF grant AST-9529098, and the Medium Deep Survey, which was funded by STScI grant GO6951 and daughters.

REFERENCES

Abraham, R. G., Ellis, R. S., Fabian, A. C., Tanvir, N. R., Glazebrook, K. 1999, MNRAS, 303, 641
 Bressan, A., Chiosi, C., Tantalo, R. 1996, A&A, 311, 425
 Bruzual, A. G., and Charlot, S. 1993, ApJ, 405, 538
 Bushouse, H., Dickinson, M., van der Marel, R. P. *et al.* 2000, ADASS, 216
 Carlberg, R. G. 1984, ApJ, 286, 403
 Carollo, C. M., Danziger, I. J., Buson, L. 1993, MNRAS, 265, 553
 Charlot, S., Worthey, G., & Bressan, A. 1996, ApJ, 457, 625
 Cowie, L. L., *et al.* 1994, ApJ, 434, 114
 Fisher, D., Franx, M., & Illingworth, G. 1995, ApJ, 448, 119
 Franx, M., & Illingworth, G., 1990, ApJ, 359, L41
 Gonzalez, J. J., 1993, PhD Thesis Univ. of Calif., Santa Cruz
 Henry, R. B. C., & Worthey, G. 1999, PASP, 762, 919
 Holtzman, J. A., *et al.* 1995, PASP, 107, 1065
 Im, M., *et al.* 2001a, ApJ, in press
 Im, M., *et al.* 2001b, AJ, 122, 750
 Im, M., *et al.* 1995, ApJ, 441, 494
 Jorgensen U.G. 1997, MNRAS, 288, 161
 Kobayashi, C. & Arimoto, N. 1999 ApJ, 527, 573
 Kormendy, J., & Djorgovski, S. 1989, ARA&A, 27, 235
 Krist 1993, ADASS II, 52, eds. Hanish, R.J., Brissenden, R.J.V., and Barnes, J. (A.S.P. Conference Series), p. 536.
 Lee, H., Yoon, S., & Lee, Y. 2001, astro-ph/0104129
 Maraston, C., & Thomas, D. 2000, ApJ, 541, 126
 Menanteau, F., Abraham, R. G., Ellis, R. S. 2001, MNRAS1, 1
 Monroe, B., & Bergeron, E. 1999, STScI ISR 99-011
 Peletier, R. F., Davies, R. L., Illingworth, G. D., Davis, L. E. & Cawson, M. 1990a, AJ, 100, 1043
 Peletier, R. F., Valentijn, E. A., & Jameson, R. F. 1990b, A&A, 223, 62
 Ratnatunga, K., Griffiths, R.E., Ostrander, E.J. 1999, AJ, 118, 86
 Rhodes, J. *et al.* 2001, ApJ, 552, L85
 Saglia, R. P. *et al.* 2000, A&A, 360, 911
 Schultz, A. *et al.* 2001, “Nimcos Instrument Handbook”, Version 4.1
 Simard *et al.* 2001, in preparation
 Tamura, N., Kobayashi, C., Arimoto, N., Kodama, T., Ohta, K. 2000 AJ, 119, 2134.
 Tantalo, R., Chiosi, C., & Bressan, A. 1998, A&A, 333, 119
 Trager, S. C., Faber, S. M., Worthey, G., Gonzalez, J. J. 2000, AJ, 119, 1645
 Worthey, G. 1994, ApJS, 95, 107

TABLE 1
 BASIC DATA FOR EARLY-TYPE SAMPLE

Object ID (1)	RA (2)	DEC (3)	z (4)	Type (5)	H (6)	I (7)	V (8)	$(B/T)_I$ (9)	r_{hl}'' (10)	R_I (11)
GSS052.6543	14:17:48.2	52:31:17.3	0.756	S0	18.02 \pm .05	20.31 \pm .01	22.26 \pm .04	0.44 \pm .01	0.637 \pm .03	0.07
GSS044.1570	14:18:04.8	52:30:59.1	0.89 \pm 0.15*	E/S0	18.96 \pm .18	21.76 \pm .04	23.79 \pm .07	0.71 \pm .06	0.175 \pm .039	0.06
GSS044.1676	14:18:04.9	52:30:53.6	0.90 \pm 0.15*	E/S0	19.82 \pm .10	22.29 \pm .05	24.33 \pm .10	0.56 \pm .13	0.195 \pm .061	0.04
GSS053.6418	14:17:55.6	52:31:52.4	0.675	Sp,S0	18.37 \pm .07	20.97 \pm .01	22.66 \pm .02	0.72 \pm .03	0.354 \pm .015	0.04
SSA13 #55	13:12:19.3	42:45:01.2	1.03	S0	18.53 \pm .21	21.82 \pm .22	N/A	0.63 \pm .35	0.379 \pm .012	N/A
GSS082.6533	14:17:28.8	52:27:37.8	0.462	E/S0	18.45 \pm .16	20.57 \pm .01	22.04 \pm .01	0.41 \pm .02	0.207 \pm .010	0.05

Note. — (1) Source ID given by FFC-XXYY, where FF is the Groth Strip subfield, C is the WFPC2 chip number, and XX and YY are the chip coordinates in units of 10 pixels. The “SSA” denotes that the object is from the Hawaii Deep Field. (2) Right Ascension (J2000). (3) Declination (J2000) (4) Spectroscopic redshifts (5) Morphological type (6)-(8) Total magnitudes for H , I , and V -bands. (9)-(11)Bulge-to-total ratio, half-light radius, and residual parameter within 2 r_{hl} for the I -band data as measured by GIM2D (Simard *et al.* 2001 in preparation).

* Photometric redshifts are derived as described in Im *et al.* (2001a)